Modified αA Crystallin in the Retina: Altered Expression and Truncation with Aging†

Rebecca J. Kapphahn,‡ Cheryl M. Ethen,§ Elizabeth A. Peters,‡ LeeAnn Higgins,§ and Deborah A. Ferrington*,‡

Departments of Ophthalmology and Biochemistry, Molecular Biology and Biophysics, University of Minnesota, Minneapolis, Minnesota 55455

Received May 13, 2003; Revised Manuscript Received October 20, 2003

ABSTRACT: Crystallins are small heat shock proteins with chaperone function that prevent heat- and oxidative stress-induced aggregation of proteins. This is the first report describing modifications of αA crystallin in the sensory retina, including altered content and truncation with aging. Proteins from adult, middle age, and old Fischer 344 Brown Norway rats were compared. Western immunoblotting was used to evaluate αA crystallin content and identify protein spots on two-dimensional gels containing αA crystallin. The type and site of multiple post-translational modifications were identified by mass spectrometry. We found the content of αA crystallin was significantly decreased in the oldest rats. On two-dimensional gels, retinal crystallins resolved into multiple spots with altered migration, indicative of changes in intrinsic charge and/or truncation. Post-translational modifications that were identified included oxidation, phosphorylation, deamidation, acetylation, and truncation. In samples from rats of all ages, a highly modified N-terminus containing these modifications was found. We also observed an age-dependent difference in the extent of N- and C-terminal truncation. These results suggest that protection against stress-induced protein aggregation is compromised in the aged retina.

αA crystallin is a member of the small heat shock protein superfamily whose members function as chaperones by preventing heat- and oxidative stress-induced aggregation of proteins (*1*). This protein was first described in the lens, where it is found in high abundance (*2*). Expression of αA crystallin in extra-lenticular tissues, including the brain, liver, spleen, thymus, heart, and retina, has subsequently been described (*3*−*6*).

The αA crystallin monomer is an ∼20 kDa polypeptide that forms multimeric complexes of ∼800 kDa with αB crystallin, a closely related protein whose sequence is 55% homologous (*7*). αA crystallin consists of several regions shown to contribute to its chaperone-like activity. The flexible, solvent-exposed C-terminal extension, composed of the last eight amino acids, maintains solubility and binds charged residues of unfolding proteins (*8*, *9*). The N-terminus binds hydrophobic amino acids that become solvent-exposed in unfolding polypeptide chains (*7*). In addition to the N- and C-termini, recent evidence has shown that select residues of the α-crystallin domain (residues 70−88) bind unfolded proteins and prevent their aggregation (*10*).

A combination of hydrophobic and ionic interactions is also required for protein stability and oligomeric complex formation. For example, residues 109−120 are part of a *β*-sheet that forms salt bridges and hydrogen bonds with other proteins in the oligomeric assembly (*11*). Thus, altering the charge of residues at the subunit interface can disrupt protein−protein interactions. *In vitro* studies on chemically modified αA crystallin and studies using site-directed mutagenesis have demonstrated that either alterations of intrinsic charge and hydrophobicity or truncation of the N- or C-termini will inhibit chaperone function (*8*, *12*−*17*).

One of the mechanisms for altering the intrinsic charge or hydrophobicity of a protein is post-translational modification (PTM)[1] of amino acid residues. Extensive PTM of crystallins from the lens has been well documented (reviewed in refs *7* and *18*). Moreover, the extent of modification has been correlated with aging. Crystallin PTM results in multiple protein species that have been separated by either chromatography (*19*) or two-dimensional (2D) polyacrylamide gel electrophoresis (*20*). Mass spectrometric analysis has been used to identify both the type, and occasionally the site, of PTM. The PTMs reported to increase with aging in lenticular αA crystallin include deamidation, acetylation, oxidation of

† This work was supported by National Institutes of Health NIA Grant RO3 AG19024, the Foundation Fighting Blindness, the American Federation for Aging Research, and an unrestricted grant to the Department of Ophthalmology from the Research to Prevent Blindness Foundation. C.M.E. was supported by NIH/NEI Grant T32 EY07133-12 and a Glenn/AFAR Scholarship from the American Federation for Aging Research.

* To whom correspondence should be addressed: Department of Ophthalmology, 380 Lions Research Building, 2001 6th St. SE, University of Minnesota, Minneapolis, MN 55455. Telephone: (612) 624-8267. Fax: (612) 626-0781. E-mail: ferri013@umn.edu.

‡ Department of Ophthalmology.

§ Department of Biochemistry, Molecular Biology and Biophysics.

[1] Abbreviations: ABI, Applied Biosystems, Inc.; ANOVA, analysis of variance; BCA, bicinchoninic acid; BCIP-NBT, 5-bromo-4-chloro-3′-iodolyl phosphate *p*-toluidine/nitro blue tetrazolium chloride; CAM, carboxyamidomethylated; DTT, dithiothreitol; ESI, electrospray ionization; F344BN, Fischer 344 Brown Norway; HSP, heat shock protein; IEF, isoelectric focusing; IPG, immobilized pH gradient; MALDI-TOF, matrix-assisted laser desorption ionization time-of-flight; MS, mass spectrometry; pI, ioselectric point; PTM, post-translational modification; PVDF, polyvinylidene difluoride; SDS−PAGE, sodium dodecyl sulfate−polyacrylamide gel electrophoresis; 1D, one-dimensional; 2D, two-dimensional.

10.1021/bi034774e CCC: $25.00
Published on Web 12/06/2003

methionine, phosphorylation, and cleavage of the N-terminal and/or C-terminal residues (*12*, *20*−*24*). Importantly, many of these modifications have been shown to inhibit chaperone function. Thus, in the aged lens, chaperone function of αA crystallin is inhibited.

To date, there have been no investigations of retinal αA crystallin expression or PTMs with aging. The retina is particularly prone to oxidative stress due to the combined effect of high metabolic activity, light-induced generation of free radicals, and membranes containing high concentrations of easily oxidized polyunsaturated fatty acids (*25*−*27*). Therefore, maintenance of chaperone function is crucial for protecting retinal proteins from oxidation-induced unfolding. In aged rat retina, we have reported increased levels of proteins containing the oxidative modifications, nitrotyrosine and 4-hydroxy-2-nonenal (*28*). These results are consistent with a more stringent requirement for protection from oxidation-induced aggregation in the aged retina.

In this study, we investigated retinal αA crystallin expression and PTMs in mature adult, middle age, and old rats. These ages were chosen so that we could capture changes at the molecular level that correlate with the sharp functional decline in the retina that occurs late in life. This study provides a comprehensive view of the time-dependent changes in αA crystallin. Precise protein modifications that occur with normal aging have not been systematically explored. Understanding the molecular nature of the aging process will provide important insight into the basis of cellular and organismal senescence.

We used a combination of high-resolution 2D gel electrophoresis and mass spectrometry (MS) to identify the types and sites of PTM. We found retinal αA crystallin contains a large number of PTMs, including an age-dependent difference in the extent of both N- and C-terminal truncation. Additionally, we found that αA crystallin content is significantly decreased with aging. These results suggest that protection from stress-induced protein aggregation is compromised in the aged retina.

EXPERIMENTAL PROCEDURES

Preparation of Retinal Homogenates. Male Fischer 344x Brown Norway (F344BN) F1 hybrid rats were purchased from the colony maintained by the National Institute of Aging (Harlan, Indianapolis, IN). Ages of rats included in this study were 7−12 months (mature adult), 28−30 months (middle age), and 32−37 months (old). Rats were housed in an AAALAC-approved animal facility at the University of Minnesota, which is maintained at 20 °C with 12 h cycles of light and dark. Standard rat chow and water were provided ad libitum. An animal protocol was approved by the Institutional Animal Care and Use Committee of the University of Minnesota and followed the guidelines established by the National Institutes of Health.

Prior to eunucleation of the eye, rats were euthanized by administering an intraperitoneal overdose of Buthanasia (100 mg/kg). The eye was removed, and an incision was made around the circumference to permit removal of the lens and vitreous humor. The eyecup was then rinsed in phosphate-buffered saline, and the sensory retina was dissected and immediately processed as outlined previously (*28*). The retinas of two rats were used for each preparation. The supernatant containing soluble retinal proteins from the final step of processing was retained, and aliquots were stored at −80 °C. Protein concentrations were determined using the bicinchoninic acid (BCA) protein assay reagents (Pierce). Bovine serum albumin was used as the standard protein.

One-Dimensional (1D) Gel Electrophoresis. Prior to Western immunoblotting to determine the relative content of crystallin and rhodopsin proteins, retinal proteins were electrophoretically separated by SDS−PAGE using a Mighty Small SE 250 (Hoeffer) system and a 12% resolving gel with a 3% stacking gel (*29*). Protein loads for preparations from human and rat retina were 10 μg per lane. The protein load for human recombinant αA crystallin (kindly supplied by M. Petrash) was 0.5 μg per lane. The relative content of crystallin was also determined with an additional antibody that reacts with the N-terminus of αA, but also has some cross-reaction with αB crystallin. For these measurements, resolution of αA and insert crystallins from αB crystallin required the use of large format gels (16 cm × 18 cm) for SDS−PAGE (Pharmacia Hoeffer). Ten micrograms of protein was loaded for each sample.

2D Gel Electrophoresis. First-dimension isoelectric focusing (IEF) was performed with the Protean IEF Cell (Bio-Rad) using 11 cm, pH 5−8 immobilized pH gradient (IPG) strips. IPG strips were rehydrated with 90 μg of rat retinal protein at 50 V for 14 h. Samples were focused at 250 V for 15 min, with a linear increase to 8000 V for 2.5 h, and a final focusing step at 8000 V to reach a total of 35 000 Vhours. For the second dimension, IPG strips were equilibrated for 10 min in buffer A [6 M urea, 2% SDS, 375 mM Tris-HCl (pH 8.8), 20% glycerol, and 130 mM DTT], followed by 10 min in buffer A with 135 mM iodoacetamide substituted for DTT. The equilibrated strips were embedded in 0.5% (w/v) agarose on the top of 12% acrylamide gels. Second-dimension SDS−PAGE was performed according to the method of Laemmli (29), using the Pharmacia Hoefer SE 600 system. For each sample, three to four gels were run in parallel. One gel was silver stained using the mass spectrometry compatible Silver Stain Plus Kit (Bio-Rad). The alternate gels were used for Western immunoblotting. Images were captured using a Fluor-S MultiImaging system (Bio-Rad).

Analysis of Protein Migration on 2D Gels. The isoelectric focusing point (pI) of crystallin proteins was determined by comparing the migration of 2D SDS−PAGE standard proteins (Bio-Rad) (conalbumin, pI 6.0, 6.3, and 6.6; albumin, pI 5.4 and 5.6; actin, pI 5.0 and 5.1; GAPDH, pI 8.3 and 8.5; carbonic anhydrase, pI 5.9 and 6.0; and myoglobin, pI 7.0) with the migration of our sample proteins. The apparent molecular mass was determined by comparing the migration of a protein spot with the position of molecular weight protein standards. For Western blots, Kaleidoscope Prestained Standards (Bio-Rad) were used. For silver-stained gels, Low Range Silver Stain SDS−PAGE Standards (Bio-Rad) were used.

Western Immunoblotting of 1D and 2D Gels. Following resolution of proteins by 12% SDS−PAGE, retinal proteins were electrophoretically transferred to polyvinylidene difluoride (PVDF) membrane using the Bio-Rad Trans-Blot Semi-Dry Cell at 800 mA for 30 min. PVDF membranes were probed with one of the following primary polyclonal

antibodies: rhodopsin (1:1000) (Biodesign, Saco, ME) or one of two different antibodies to αA crystallin. The αA crystallin antibody purchased from Stressgen (1:1000) was generated for the last 10 amino acids in the C-terminus. This sequence is identical in rats and humans except for the substitution of Ser^{168} in rat with Thr^{168} in humans. The second αA crystallin antiserum (1:750), kindly provided by J. Horwitz, was generated from a peptide that matches the first 11 amino acids in the N-terminus of bovine αA crystallin (*6*). The sequence is identical between the bovine and rat except for the two amino acids at positions 3 and 4. Following 2D gel resolution of rat retinal proteins, we observed a slight cross-reaction with αB crystallin for the antibody reacting with the N-terminus and no cross-reaction for the antibody reacting with the C-terminus. A cross-reaction between αA and αB crystallin with the antibody raised against the N-terminal sequence was reported previously (*5*, *6*).

Goat anti-rabbit alkaline phosphatase-conjugated secondary antibody (1:3000) was used in conjunction with the substrate 5-bromo-4-chlor-3′-iodolyl phosphate *p*-toluidine/nitro blue tetrazolium chloride (BCIP-NBT) to visualize the immunoreaction. Images were captured using a Fluor-S Multi-Imaging System (Bio-Rad).

To determine the relative content of αA crystallin or rhodopsin in rat retinal homogenates, densitometric analysis was performed on the immunoreaction of individual protein bands using Sigma Scan. Preliminary experiments showed that retinal protein loads between 1 and 30 μg produced a linear signal for the αA crystallin antibody. Therefore, 10 μg was chosen as the amount of total protein to load for the semiquantitative Western blot analysis. All band densities were normalized to a reference sample from an adult rat retinal homogenate that was included in each Western blot. This allowed for blot-to-blot comparisons. The density is reported as the immunoreaction relative to the average density of young rat retinal crystallin. Differences between age groups were tested for statistical significance using a one-way analysis of variance (ANOVA), with the level of significance (p) set at ≤ 0.05. When appropriate, post hoc analysis was performed using the Tukey−Kramer statistical test to determine differences between groups.

To determine the extent of either N- or C-terminal truncation using 2D gel resolution, densitometric analysis was performed on the immunoreaction of each protein spot. The relative percent of truncation was determined by dividing the density of the truncated species by the total density of all αA crystallin immunoreactions on the blot.

Selection and Preparation of Proteins for Mass Spectrometry. Western immunoblotting of 2D gels was used to identify protein spots containing αA crystallin. To align spots exhibiting an immunoreaction with spots on silver-stained gels, images of Western immunoblots and their corresponding gels were printed on transparencies and overlaid on a light box. Selected spots were excised and proteins digested in-gel overnight at 37 °C with either trypsin or AspN as described previously (*30*). Prior to protease digestion, the cysteine residues were reduced with DTT and alkylated using iodoacetamide. Peptides were extracted from gels by repeated swelling and shrinking of the gel using a 1:1 (v/v) mixture of 25 mM ammonium hydrogen carbonate and acetonitrile, followed by a 1:1 (v/v) mixture of 5% formic acid and acetonitrile (*31*). Extracted peptides were evaporated to near dryness in a Speed Vac and stored at −80 °C prior to mass spectral analysis.

Methyl Esterification of Peptides. Following enzymatic digestion with trypsin, dried peptides were treated with a methanolic hydrochloride solution that was prepared fresh by adding 160 μL of acetyl chloride dropwise with stirring on ice to 1 mL of anhydrous methanol (*32*). The mixture was then removed from ice and stirred at room temperature for 10 min. Fifty microliters of the methanolic hydrochloride solution was added to each sample of dried peptides, and the mixtures were incubated at room temperature for 2 h. The solvent was removed and the reaction stopped by complete drying of peptides in a Speed Vac. This treatment results in the addition of 14 mass units to the C-terminus and side chains of aspartic acid and glutamic acid resulting from the chemical addition of an ester group. Deamidation at asparagine and glutamine residues to their corresponding acid derivatives can be detected because they form methyl esters, which is observed as an increase of 15 mass units (+1 due to deamidation and +14 due to esterification).

Matrix-Assisted Laser Desorption Ionization Time-of-Flight Mass Spectrometry (MALDI-TOF MS). Prior to MALDI-TOF MS analysis, a portion of the peptide mixture was desalted using Millipore C18 ZipTips using the manufacturer's protocol. Full scan mass spectra from m/z 500 to 3500 of the tryptic peptide mixtures were collected in the positive mode by averaging ∼50−200 spectra, depending on the instrument. Data were acquired on one of the following mass spectrometers: Brüker Biflex III (Brüker Daltonics, Billerica, MA), QSTAR Pulsar quadrupole-TOF [Applied Biosystems Inc. (ABI), Foster City, CA], or QSTAR XL quadrupole-TOF (ABI). For Biflex MS, the mass spectrometer is equipped with an N_2 laser (337 nm, pulse length of 3 ns). The peptide data were collected in the reflectron mode, with an accelerating potential of 19 kV using α-cyano-4-hydroxycinnamic acid (cca) (Agilent Technologies, Palo Alto, CA) diluted 1:1 (v/v) with a 50:50 acetonitrile/Nanopure water mixture and 0.1% trifluoroacetic acid. External calibration was performed using human angiotensin II (monoisotopic [MH^+] of m/z 1046.5417; Sigma), angiotensin I (monoisotopic [MH^+] of m/z 1296.6853; Sigma), and adrenocorticotropin hormone fragment 18−39 (monoisotopic [MH^+] of m/z 2465.1989; Sigma). For QSTAR Pulsar MS, full scan and product ion spectra were collected using dihydroxybenzoic acid as the matrix. The TOF region acceleration voltage was 4 kV, and the injection pulse repetition rate was 6.0 kHz. Laser pulses were generated with a nitrogen laser at 337 nm, with 33 μJ of laser energy using a laser repetition rate of 20 Hz. For QSTAR XL MS, the TOF region acceleration voltage was 4 kV and the injection pulse repetition rate was 6.0 kHz. Laser pulses were generated with a nitrogen laser at 337 nm, with ∼9 μJ of laser energy using a laser repetition of 20 Hz and cca as the matrix. To increase the accuracy of the m/z values, internal calibration for the QSTAR data was performed using peptides of either trypsin autolysis ([MH^+] of m/z 842.5022 and 2211.0968) or αA crystallin ([MH^+] of m/z 1007.5314 and 1285.6798). The identities of the internal calibrants were previously confirmed by MS/MS sequencing. The internal standard for each sample was chosen on the basis of peak intensity (the more intense peaks were chosen as calibrants).

After internal calibration, the ABIs Bayesian Peptide Reconstruct Tool, which is very robust since multiple peaks in an isotope series are used during the Bayesian calculation, was used to generate a peak list for sample peptides.

Measured peptide masses were used to search the NCBI and Swiss-Prot sequence databases for protein identifications and database accession numbers using Mascot (www.matrixscience.com) or BioAnalyst (ABI) software. All searches were performed with a mass tolerance between 50 and 175 (for QSTAR data) and 100 and 225 ppm (Biflex). Positive identification required a minimum of three peptide matches, a probability score that indicates high concordance between the masses of experimentally derived peptides and theoretical masses of peptides from the matched protein, and a positive identification from at least one product ion spectrum.

Electrospray Ionizaation (ESI) Mass Spectral Analysis. An LCP (LC Packings, Sunnyvale, CA) Famos autosampler aspirated 30 μL of an acidified (with 0.1% formic acid) peptide mixture into a 100 μL sample loop using the Famos micoliter pick-up injection mode and a combination of a 98:2 water/ACN mixture and 0.1% formic acid as the transfer reagent. An LCP Switchos pump was used to concentrate and desalt the sample on an LCP C18 nano-precolumn [0.3 mm (internal diameter) × 1 mm (length)] with a combination of a 98:2 water/ACN mixture and 0.1% formic acid as the buffer. The precolumn was switched in-line with an analytical column, and peptides were eluted at 350 nL/min using an LCP Ultimate LC system. A 100 μm internal diameter C18 column was packed in-house to 10 cm length with 5 μm particles, with a pore size of 200 Å (Michrom BioResources, Auburn, CA) (*33*). Peptides were eluted with a linear gradient of 1.6% solvent B/min over 65 min starting with 100% solvent A, where solvent A was a 95:5 water/ACN mixture with 0.1% formic acid and solvent B was a 5:95 water/ACN mixture with 0.1% formic acid. The LC system was on-line with ABI's QSTAR Pulsar quadrupole-TOF MS instrument, which was equipped with Protana's (Denmark) nano-electrospray source. A spray voltage of 2100 V was applied distal to the analytical column. TOF parameters are the same as the parameters listed above for the QSTAR Pulsar instrument equipped with the MALDI source. Product ion spectra were collected in an information-dependent acquisition mode using the enhanced feature of the scan mode with a scan time of 3 s.

Identification of Post-Translational Modifications (PTM). Peaks whose mass matches that of peptides containing potential PTMs were identified by either manually searching the peptide mass list or using the software tool FindMod (http://us.expasy.org/tools/findmod/). In FindMod, the experimentally measured peptide masses are compared with the theoretical masses of peptides from the identified protein. The mass differences between experimental and theoretical peptides are used to predict the type of modification that could correspond to the mass change. A prediction of the site of modification is determined by algorithms in the software that are based on biochemical principles for modification of specific amino acids. (*34*). Mass accuracy in parts per million (ppm) was calculated to check the validity of the prediction. The ppm value was determined by dividing the difference between the experimental and theoretical *m*/*z* values by the theoretical *m*/*z* value. The quotient is then multiplied by 10^6. Confirmation of one PTM (see Results) was accomplished by tandem mass spectrometry.

RESULTS

The Level of Crystallin Expression Decreases with Aging. In this study, we investigated αA crystallin protein expression and PTM in the sensory retina. The sensory retina contains the rod and cone photoreceptors and six other neuronal and support cells that are involved in processing and transmitting visual information to the brain. To identify age-dependent changes in αA crystallin, we compared protein from mature adult (7−12 months), middle age (28−30 months), and old (32−37 months) F344BN rats. On the basis of the published life span for this rat strain, these ages correspond to (1) ∼95% survival for the mature adult group, (2) 70−60% survival, just prior to senescence, for the middle age group, and (3) 50−20% survival, well into senescence, for the old group (*35*). Thus, this study is focused on understanding changes that occur later in life, rather than during development of the young organism.

To evaluate the relative content of αA crystallin, Western immunoblotting was performed on retinal proteins separated by 1D SDS−PAGE using an antibody that specifically recognizes the C-terminus of αA crystallin (Figure 1A). The specificity of this antibody was confirmed by the selective reaction with protein spots on 2D gels whose identity was confirmed by mass spectral analysis (see below). We observed a single immunoreactive band migrating at ∼20 kDa for recombinant human αA crystallin and in retinal homogenate from a human donor eye. This apparent mass is in good agreement with the theoretical molecular mass of 19 909 Da for human αA crystallin (*36*). In rat retinal homogenates, two protein bands reacted with the antibody. The band with the strongest reaction migrated slightly faster than the human αA crystallin, reflecting the smaller mass, i.e., 19 792 Da, for rat αA crystallin. The second band at ∼22 kDa corresponds to an alternate gene product, αA insert crystallin (henceforth termed αA insert), that was previously described in the rodent lens (*37*). This protein product arises from alternative splicing of mRNA, producing a protein with a 23-amino acid insert between residues 63 and 64 of αA crystallin (*38*).

Densitometric analysis of the two immunoreactive protein bands in rat retinal homogenates indicates that there is an age-dependent loss in both αA crystallin and αA insert (Figure 1B). In old rats, the crystallin content is significantly decreased 40 and 60% for αA crystallin and αA insert, respectively, compared with adult rats.

To determine if the age-dependent decrease in content occurs at equivalent rates for both species of crystallin, we calculated the ratio between αA insert and αA crystallin immunoreaction. Since the C-terminus is identical for both αA insert and αA crystallin, the affinity of the antibody used to evaluate relative content should be the same for both proteins. In adult retina, the content of αA insert is approximately 25% lower than the content of αA crystallin. In middle age and old rats, the relative concentration of αA insert is ∼50 and 70% less, respectively, than the concentration of αA crystallin. Thus, there is a more substantial loss in αA insert with aging.

To ensure that these results were not biased by differences in C-terminal truncation, we used an alternative antibody that

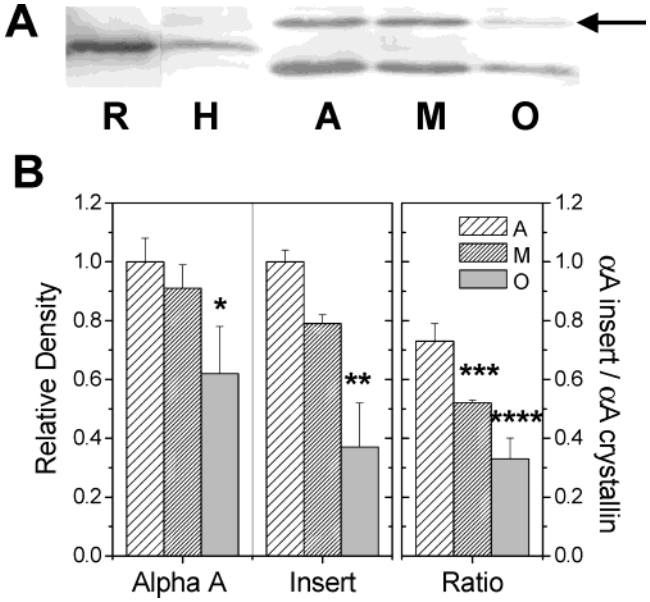

FIGURE 1: Western immunoblot analysis of αA crystallin content in adult (A), middle age (M), and old (O) rat retina. (A) Representative Western blot for the reaction of an antibody that recognizes the C-terminus of αA crystallin with recombinant human αA crystallin (R), and in human (H) and rat retinal homogenates (A, M, and O). Protein loads were 0.5 μg of recombinant protein and 10 μg of retinal homogenates. The arrow indicates the position of αA insert. (B) The relative amount of αA crystallin in retinal homogenates was determined from densitometric analysis of the immunoreactions for αA crystallin (Alpha A) and αA insert (Insert). Plots summarize the mean (±standard error) of densitometric values from each band that were normalized to the immunoreaction in a standard sample from adult rat retina (left and middle panels). The right panel shows the ratio of the relative content of αA insert to αA crystallin for each age group calculated from the normalized densitometric values. $N = 10$ for adult and old samples and 7 for middle age samples. One asterisk means $p = 0.04$. Two asterisks mean $p = 4.0 \times 10^{-4}$. Four asterisks mean $p = 3.0 \times 10^{-4}$ (significantly different between young and old rats). Three asterisks mean $p = 0.04$ (significantly different between young and middle age rats).

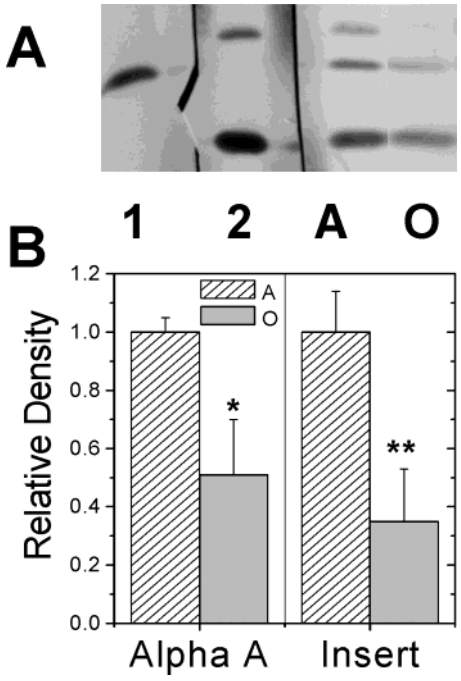

FIGURE 2: Confirmation of αA crystallin content by Western immunoblots of adult (A) and old (O) retina using an alternative antibody. (A) Representative Western blot of the immune reaction of rat retinal homogenate to the following antibodies: (1) αB crystallin, (2) C-terminus of αA crystallin, and (A and O) N-terminus of αA crystallin. (B) Plots summarizing densitometry of the mean (±standard error) immune reaction in adult and old rats for αA crystallin (Alpha A) and αA insert (Insert), normalized to the immunoreaction in a standard sample from adult rat retina. $N = 5$ per age group. One asterisk means $p = 0.05$. Two asterisks mean $p = 0.02$.

recognizes the N-terminus to supplement and confirm the age-dependent decrease in the extent of the immune reaction. However, this antibody exhibits some cross-reaction with αB crystallin, so we solved this problem by separating retinal proteins via large format 1D SDS−PAGE prior to incubation with the antibody. As shown in Figure 2A, this approach clearly resolved the protein bands containing αA and αA insert from αB crystallin. We used the protein specific immune reactions of antibodies to either αB crystallin (lane 1) or the C-terminus of αA crystallin (lane 2) as our guide in determining the correct band to chose for densitometry for each αA crystallin species. Using the antibody that reacts with the N-terminus, we observed a significant decrease in the extent of antibody reaction to both αA and αA insert when comparing the reaction in young adult and old rats (Figure 2B). The combined results using two antibodies that recognize different epitopes on the protein confirm that there is a decreased content of retinal αA and αA insert crystallin with aging.

Immunohistochemistry has shown that the α-crystallins are present in the photoreceptor cells of the sensory retina (*4*, *39*). Since a 20−35% decrease in photoreceptor density has been reported in pigmented rats with aging (*40*, *41*), we asked if the age-dependent loss of photoreceptors could account for the ∼50% decrease in αA crystallin content in our oldest animals. Therefore, we measured the relative content of rhodopsin, the major protein constituent of the rod outer segments of photoreceptors, by Western immunoblotting (Figure 3). Densitometric analysis of the immunoreactive band showed an age-dependent decrease in rhodopsin content. The extent of immunoreaction in old rats decreased 30% compared with that in adult and middle age rats. These results are consistent with an age-dependent loss in photoreceptors. However, the age-related loss in αA crystallin content is still proportionately greater than the loss in photoreceptors, suggesting an overall decline in retinal αA crystallin content.

Identification of Crystallin Proteins by Western Immunoblotting. To investigate αA crystallin PTMs, we utilized 2D gel electrophoresis to resolve individual proteins in the complex mixture of retinal proteins. This technique also resolves modified proteins that differ in their intrinsic charge from the "parent" or unmodified protein. Following 2D separation of retinal proteins, protein spots containing either αA crystallin or αA insert were identified by a combination of immunochemical detection on Western blots and mass spectral analysis. Figure 4 shows a representative immunoreaction of the αA crystallin antibodies that recognize either the N- or C-terminus and the corresponding 2D silver-stained gel for retinal proteins from adult (A−C), middle age (D−F), and old (G−I) rats.

When probing immunoblots of 2D gels with an antibody that recognizes the C-terminus of αA crystallin, we found

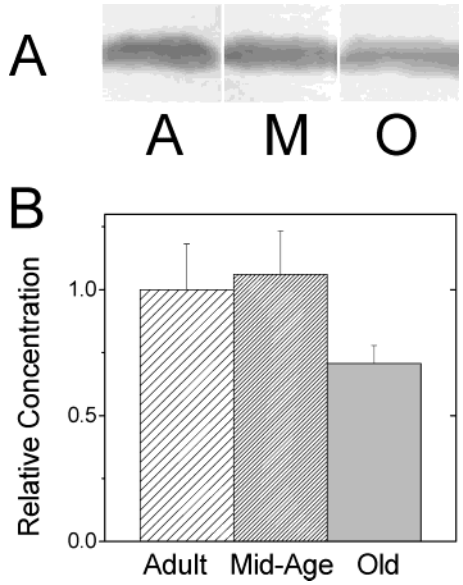

FIGURE 3: Comparison of rhodopsin expression in adult (A), middle age (M), and old (O) rat retina. (A) Representative Western blot for the reaction of rhodopsin antibody with rat retinal homogenates (A, M, and O). Protein loads were 10 μg of retinal homogenates. (B) The relative amount of rhodopsin in retinal homogenates was determined from densitometric analysis of the immunoreactions. Plots summarize the mean (±standard error) of densitometric values from each band that were normalized to the immunoreaction in a standard sample from adult rat retina. $N = 5$ per age group.

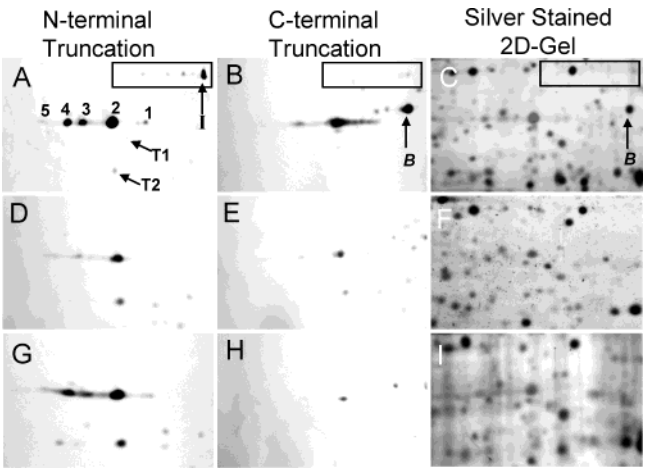

FIGURE 4: Identification of αA crystallin and αA insert in retinal proteins resolved by two-dimensional polyacrylamide gel electrophoresis. Proteins from retinal homogenates (90 μg) were resolved by isoelectric focusing on an immobilized strip with a linear pH gradient (pH 5 to 8) in the first dimension, and then by SDS−PAGE (12%) in the second dimension. Three gels per sample were run in parallel. Two gels were used for Western immunoblotting using an antibody to αA crystallin that recognizes either the C-terminus (A, D, and G, labeled N-terminal Truncation) or the N-terminus (B, E, and H, labeled C-terminal Truncation). The third gel was stained with silver (C, F, and I, labeled Silver Stained 2D-Gel). Each panel is a portion of a 2D gel from pI 5.4 to 7.2 and from an M_r of 12 kDa to an M_r of 23 kDa. Numbers indicate the major αA species in adult (A−C), middle age (D−F), and old (G−I) rat retina (numbering is in panel A only). Arrows indicate the immune reaction corresponding to truncated αA crystallin, T1 and T2 (A, D, and G). Boxed protein spots are αA insert. A spot of αA insert identified by MS is indicated with an arrow and I. Cross-reaction with a protein spot of αB crystallin that was verified by MS analysis is indicated by *B* (B and C).

the major reaction was present in five protein spots that migrated at ~19.5 kDa, but with isoelectric points (pI) between 5.8 and 6.6 (Figure 4A,D,G). Multiple spots at different pIs for the same protein are known as "charge trains", which result from PTMs that alter the intrinsic charge of the protein. When the intensity of the reaction of the major spots was compared, spot 2 was the most abundant αA species in all age groups. Spots 1 and 5 were present in very low relative concentrations. In some samples, spot 5 was not detected at all.

In adult retina, we observed a second reaction that was at ~22 kDa and more basic than the reaction for αA crystallin (Figure 4A−C, box). This pattern of migration is consistent with the theoretical values for migration of αA insert, i.e., 22 447 Da and pI 6.35. The αA insert also appears as a charge train, suggesting that this protein undergoes PTM. In the old retina, a reaction for αA insert was rarely visible.

The most striking difference in the immune reaction was the age-related increase in the number of immunoreactive proteins migrating at a mass lower than those of the five major crystallin proteins (Figure 4). These immune reactions at lower molecular mass are likely associated with truncated αA crystallin proteins. Since this polyclonal antibody was generated using a peptide matching the sequence of the last 10 C-terminal amino acids, truncation must be from the N-terminus for these immunoreactive protein spots. Densitometric analysis of the immune reaction showed 3 ± 1, 14 ± 13, and 27 ± 1% of the total reaction was associated with the truncated protein in young, middle age, and old retinas, respectively. As demonstrated by the large error associated with these measurements in young and middle age retinas, there was considerable variability between samples. However, by advanced age, the relative amount of truncation is fairly constant. Two truncated proteins, T1 and T2, were found in all ages, but the relative content between samples varied considerably. Migration of T1 is at ~18 kDa and basic to spot 2. The truncated protein, T2, migrates at ~15 kDa and at the same pI as spot 2. The change in the apparent mass from the parent protein suggests a loss of ~50 residues. While T2 was present even in retinal samples from young adults, the more intense immune reaction in older rat retina suggests an increased abundance with aging.

The immunoreaction of a Western blot performed in parallel using a second antibody that recognizes the first 11 amino acids of the N-terminus of αA crystallin is also shown (Figure 4B,E,H). Thus, this antibody should recognize αA crystallin containing C-terminal truncations. Spots 2−4 and the reaction for αA insert are visible, although the extent of the immune reaction was significantly less than that of the previous antibody. Additionally, there was some cross-reaction with αB crystallin (indicated as *B*). However, the difference in migration on 2D gels allows for clear resolution of the different crystallin proteins. In adult and middle age retinas, several truncated species were present and made up ~14 ± 10 and 10 ± 10% of the total immune reaction, respectively. As with the N-terminal truncation, there was significant variability in the extent of truncation between samples. These results are consistent with the presence of both N- and C-terminal truncation in retinal αA crystallin in adult and middle age rats. In striking contrast, no immunoreactions were visible for proteins of <19 kDa in the oldest age group. These results suggest that the C-terminal

truncations in the oldest age group were either absent or below the level of detection for this antibody.

Confirmation of Identity by Mass Spectrometry. We performed peptide mapping using full scan MALDI-TOF MS data to confirm the identity of the immunoreactive spots and search for PTMs. Tandem MS data were acquired (by MALDI or ESI using QSTAR mass spectrometers) to provide peptide amino acid sequence information and unambiguous confirmation of a protein's identity. Figure 5A shows a representative MALDI-TOF mass spectrum of peptides generated from in-gel trypsin digestion for a protein spot that was identified as αA crystallin (spot 2). Eighteen peptides representing 86% of the primary sequence for αA crystallin were identified from the peptide mass fingerprint (Table 1). In this sample, six peptides were sequenced by tandem MS, thus providing unambiguous identification of the protein.

The fragmentation of two peptides from residues 13−21 (peptide 1007) and 89−99 (peptide 1285) of αA crystallin is shown in the MS/MS spectra in Figure 6. These two peptides were well-defined peaks in most samples with signal-to-noise ratios of >10 and were used as internal calibration standards for determining the *m*/*z* values for other peptides found in that sample. The fragmentation of peptide 1007 produced a spectrum containing 6 of 9 b ions and 8 of 9 y ions (Figure 6A). Also identified were a number of immonium ions, neutral losses of water or ammonium, and internal fragments. The large number of internal fragmentations was due to the presence of the proline in this peptide. In the MS/MS spectrum corresponding to a peptide with an *m*/*z* value of 1285, the presence of 8 of 11 b ions and 10 of 11 y ions verified the sequence for residues 89−99 of αA crystallin (Figure 6B).

The initial identification of αA crystallin by Western blots was confirmed by MS analysis for spots 1−5, T1, and I (part of the charge train of the αA insert) (Figure 4). The cumulative sequence coverage by MALDI-TOF analysis and the number of peptides matching the primary sequence of αA crystallin are provided in Table 2. To improve our sequence coverage, we also performed MS analysis on peptides generated by AspN endoproteinase for a limited number of samples. Tandem MS was performed on 4−10 peptides for each sample to confirm the MALDI-TOF peptide map identification.

Identification of Post-Translational Modifications. Our next step was to determine the molecular basis for the altered mobility demonstrated by retinal αA crystallins. Previous investigations of crystallins in the lens have identified numerous PTMs that alter a protein's intrinsic charge and, consequently, its mobility on 2D gels. Reported charge-altering modifications include phosphorylation, acetylation or glycation of lysine, deamidation of asparagine or glutamine, and glutathionylation of cysteine (*20*−*22*, *42*). Additionally, truncation of the N- and C-termini, which contain a large number of charged amino acids, was reported to alter the migration of the protein in both dimensions on 2D gels (*20*, *22*). We used this *a priori* information from lenticular crystallins to search for similar modifications in retinal crystallins. The strategy we followed was to calculate the mass of specific peptides with their expected modification and manually search the MALDI-TOF peak list for these theoretical *m*/*z* values. The program FindMod (http//us.expasy.org/tools/findmod/findmod.html) was also used to assist in identifying peptides with potential modifications. Visual inspection of the spectra was performed to verify that the peak corresponding to the mass of a potentially modified peptide had a shape that was consistent with a peptide isotopic series pattern and had a signal-to-noise ratio of >2. To increase the accuracy of the monoisotopic masses generated on the QSTAR mass spectrometer, internal cali-

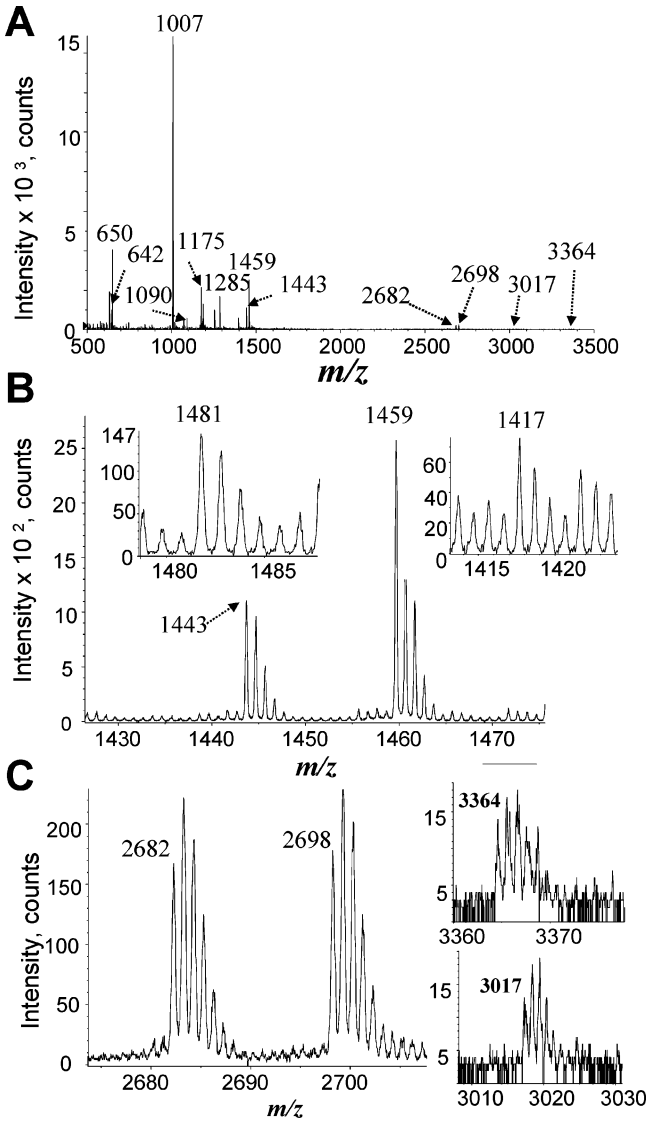

FIGURE 5: Mass spectrometric analysis of tryptic peptides from αA crystallin. (A) Full scan of a MALDI-TOF MS peptide mass fingerprint from spot 2. The spectrum shows 12 of the 15 peaks matched to the theoretical *m*/*z* values for residues in the sequence from rat αA crystallin (GenBank entry 19526477). The 15 matching peptides covered 84% of the sequence (Table 1). (B) Zoom scan of the region of the spectrum that corresponds with peptide 1−11 (MDVTIQHPWFK) with multiple modifications, including acetylation, methionine oxidation, and phosphorylation. Peptides 1417 and 1459 contain an oxidized methionine. Peptides 1443 and 1459 contain an acetyl group. Peptide 1481 is phosphorylated. The calculated mass accuracy for each peptide is provided in Table 3. (C) Zoom scan of peaks matching the *m*/*z* values for residues 22−49 (3364) (LFDQFFGEGLFEYDLLPFLSSTISPYYR), 118−145 (3017) (YRLPSNVDQSALSCSLADGMLTFSGPK), and 120−145 (2682, 2698). Peptides 2682, 2698, and 3017 include S-carboxymethylation of cysteine, the deliberate chemical modification by iodoacetamide introduced during sample processing. Peptides 2698 and 3017 also contain an oxidized methionine. The calculated mass accuracy for each modified peptide is provided in Table 3.

Table 1: Tryptic Peptides from αA Crystallin Measured by Mass Spectrometry[a]

residues	MC[b]	theoretical [M$^+$H]	sequence[c]	identification	
				TOF[d] *m*/*z*	Sq[e]
1−11	0	1417.693	M(o)DVTIQHPWFK	x	
1−11	0	1443.709	M(a)DVTIQHPWFK	x	E
1−11	0	1459.709	M(a,o)DVTIQHPWFK	x	
1−11	0	1481.678	MDVT(p)IQHPWFK	x	
13−21	0	1007.531	ALGPFYPSR	x	M
22−49	0	3364.645	LFDQFFGEGLFEYDLLPFLSSTISPYYR	x	
50−54	0	650.362	QSLFR	x	M
55−65	0	1175.627	TVLDSGISEVR	x	M
71−78	0	980.582	FVIFLDVK	x	
79−88	0	1172.595	HFSPEDLTVK	x	
89−99	0	1285.679	VLEDFVEIHGK	x	M
104−112	0	1090.491	QDDHGYISR	x	M
118−145	1	3017.439	YRLPSNVDQSALSC(c)SLSADGM(o)LTFSGPK	x	
120−145	0	2682.275	LPSNVDQSALSC(c)SLSADGMLTFSGPK	x	
120−145	0	2698.275	LPSNVDQSALSC(c)SLSADGM(o)LTFSGPK	x	
146−157	0	1255.603	VQSGLDAGHSER	x	
158−163	0	642.393	AIPVSR	x	

[a] Following in-gel trypsin digestion of αA crystallin, peptide fragments were analyzed on a QSTAR Pulsar quadrupole MALDI-TOF MS instrument. Theoretical *m*/*z* values are the monoisotopic masses. The corresponding mass spectrum is shown in Figure 4. [b] MC is the number of trypsin-missed cleavage sites in a peptide. [c] Modification indicated in parentheses, positioned C-terminal to the relevant amino acid: o, methionine oxidation; a, acetylation; c, *S*-carboxyamidomethylation of cysteine by iodoacetamide; p, phosphorylation. [d] Peptide *m*/*z* value determined by MALDI-TOF MS. [e] Peptide sequence confirmed by either ESI tandem MS (E) or MALDI tandem MS (M). The tandem mass spectra for peptides 13−21 and 89−99 are shown in panels A and B of Figure 5, respectively. The ESI tandem MS spectrum for peptide 1−11 is shown in Figure 6.

Table 2: Cumulative Percent Coverage and Modified Residues Present in Protein Spots of αA Crystallin[a]

spot no.[b]	coverage		phosphorylation[c]		deamidation[c]		acetylation[c]	oxidation[c]	
	%	peptides	Thr^4	Ser^{122}	Gln^6	Asn^{101}	Met^1	Met^1	Met^{138}
1	69	12		x	x		x	x	x
2[d]	93	18 (8)	x	x	x	x	x	x	x
3[d]	79	12 (8)	x	x	x	x	x	x	x
4	72	13	x	x			x	x	
5	50	9	x		x		x	x	x
T1	54	10		x					x
I	67	11	x	x			x	x	x

[a] Cumulative data for individual protein spots determined by MALDI-TOF MS analysis. [b] Spot numbers correspond to multiple αA crystallin protein spots on 2D gels (Figure 3). Spots 1−5 are part of the major "charge train". T1 is truncated and basic to spot 2. I is an αA insert crystallin. [c] An x indicates the presence of a peptide with a mass consistent with the addition of the indicated modification. The sites of modification were reported previously in lenticular αA crystallin. [d] Percent is the cumulative coverage for digests by both trypsin and AspN. The number of peptides generated by digestion with AspN endoprotease is shown in parentheses.

bration was performed using either peaks from trypsin autolysis or αA crystallin prior to generating a peptide *m*/*z* list. A calculated mass accuracy of ∼5 ppm has been used with a quadrupole-TOF mass spectrometer (ABI's QSTAR) to confirm agreement between theoretical and experimental masses of peptides from homologous proteins (*43*). These guidelines are extremely stringent for our study, which was performed under experimental conditions that should allow for fewer errors in matching experimental and theoretical masses. Our experimental conditions include (1) verification that each sample contains αA crystallin by MS/MS sequencing of at least four peptides prior to further analysis, (2) internal calibration and use of the peptide reconstruct tool to generate a peptide *m*/*z* list, and (3) utilizing previously published information from lenticular αA crystallin to search for specific modifications at known positions in the sequence. It is reported in the literature (*78*) that 2 ppm is the upper limit for using the mass value only (without MS/MS data) for unambiguously reporting a correct peptide match. QSTAR quadrupole-TOF mass spectrometers do not have the resolving power to provide this type of data. We believe that internal calibration, which has provided numbers of ∼10 ppm, plus additional analytical methods for the support of modifications provides strong evidence for the presence of modified peptides, which we report in this study. However, modifications where the matches are >5 ppm should be interpreted as a putative modification suggested by the peptide mass, but not yet confirmed.

For αA crystallin, two major sites of phosphorylation have been previously identified at Thr^4 and Ser^{122} (*44*, *45*). Inspection of the MALDI-TOF mass fingerprints provided evidence for phosphorylation of each site, although the peptides containing Thr^4 and Ser^{122} contained a heterogeneous mixture of additional modifications.

For the N-terminus, we found tryptic peptides with peaks consistent with residues 1−11 or 1−12 and combinations of the following modifications: phosphorylation (79.98), acetylation (42.01), methionine oxidation (15.99), and deamidation (0.98). With close inspection of each sample, the unmodified, monoisotopic peptide with an *m*/*z* 1400.69 value was never found.

Figure 5B shows a representative MALDI-TOF mass spectra for peptides 1−11 (MDVTIQHPWFK) with various modifications. Table 3 provides the calculated mass accuracies for the observed and theoretical monoisotopic mass values for the modified peptides. The peaks at *m*/*z* 1417,

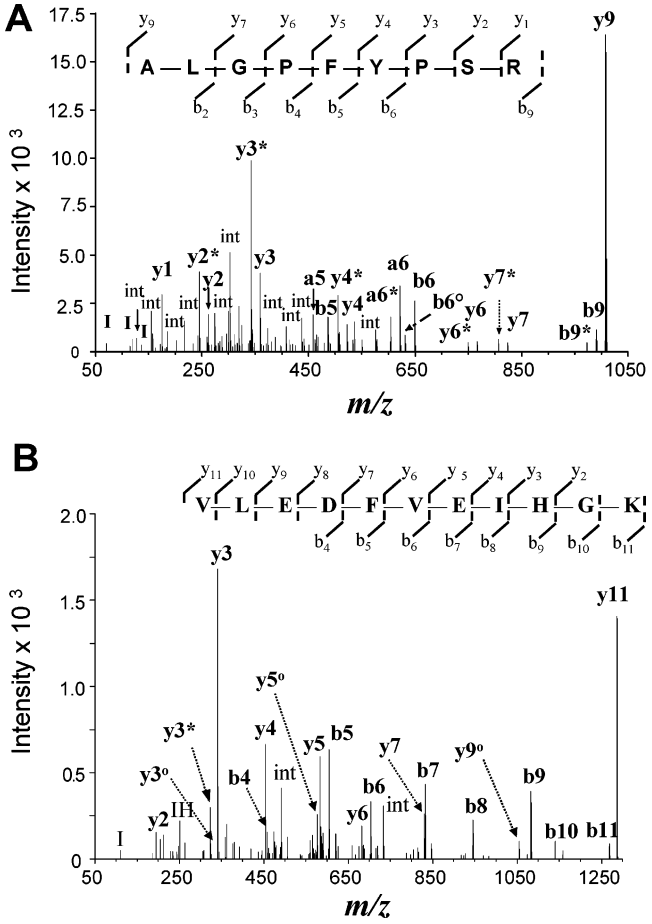

FIGURE 6: Tandem mass spectrum for fragmentation of peptides from αA crystallin used as internal standards for calibration. (A) Product ion spectrum of the singly charged ion 1007 of the ALGPFYPSR peptide formed by MALDI ionization. The amino acid sequence is displayed above the spectrum and corresponds to residues 13−21 of αA crystallin. The y- and b-type ions found experimentally are written above and below the sequence, respectively, and are indicated above the corresponding peak in the spectrum. All b and y ions cannot be shown on the spectrum because of space constraints. The asterisks denote loss of NH_3, and the degree signs denote the loss of a water from a fragment ion. Fragment ion nomenclature and neutral loss notation were established by Biemann (*77*). Our notation "int" denotes internal fragmentation, which is promoted by the presence of a proline in the sequence. Immonium ions are labeled globally with an I. The presence of NH_3 losses from a fragment ion devoid of Arg (R) or Gln (Q) from singly charged MALDI ions has been previously reported (*77*). (B) Product ion spectrum of the singly charged ion 1286 of the VLEDFVEIHGK peptide formed by MALDI ionization. The sequence matched residues 89−99 of αA crystallin. The ions are labeled as described above. The data were plotted as a function of *m*/*z* value using GraphPad Prism after the raw mass spectral data were smoothed, centroided, and labeled in BioAnalyst (ABI).

1443, and 1459 are consistent with the addition of an oxygen, acetyl group, and both modifications, respectively. Acetylation on the N-terminus of Met[1] was also confirmed by ESI-MS sequencing (Figure 7). It is important to note that we found evidence of both acetylated and nonacetylated N-terminal peptides in our samples (Table 3). This is in contrast with lenticular αA crystallin, where the N-terminal Met is always acetylated (*7*, *18*). We also observed oxidation on the side chain of Met[1], although it was unclear whether methionine oxidation occurred *in vivo* or was an artifact of sample preparation.

Another modification of the N-terminal peptide was phosphorylation of Thr[4]. While the calculated mass accuracy fell outside our accepted range of <10 ppm for the example spectrum (Figure 5), we were able to provide strong evidence of the presence of phosphorylation of the N-terminus in two other samples that had mass accuracies of 3 and 4 ppm (Table 3). Peptides with masses indicative of N-terminal phosphorylation occurred frequently, i.e., in 61% of our samples, although a mixture of both phosphorylated and nonphosphorylated peptides was often present in the same protein spot. In samples containing a mixture of phosphorylated and nonphosphorylated peptides, we also searched for a peptide mass consistent with the loss of a phosphatidic acid (*m*/*z* −98), which could potentially occur upon MALDI ionization or metastable decomposition of the peptides in the mass spectrometer. However, these peptides were not found. Thus, the mixture of phosphorylated and nonphosphorylated peptides is not the result of an artifact of sample preparation or ionization in the mass spectrometer.

Deamidation of Gln[6] in the N-terminus was more difficult to verify by our method of analysis. However, we did find evidence of deamidation of Asn[101] in our search of *m*/*z* values (Table 3).

Another method we used to establish deamidation of Gln[6] was to perform methyl esterification of peptides prior to mass spectral analysis. Methyl esterification converts the carboxyl terminus of the peptide as well as carboxylic acids, such as those present on the side chains of glutamic and aspartic acids and the deamidated side chains of glutamine and asparagine, to their corresponding methyl ester (*32*). This chemical modification results in a mass change of 15 for the deamidated residue, which greatly enhances our ability to detect this modification. We observed peptide mass additions from methyl esterification that were consistent with deamidation of peptide 1−11 (Table 3), albeit still above our desired level of mass accuracy of <10 ppm. The additional site of deamidation of Asn[101] was also observed in multiple peptides using this method, based on peptide mass alone, although the mass accuracy was ∼100 ppm. Thus, deamidation was the most difficult modification to unambiguously verify, and we were not successful in acquiring MS/MS spectra on potentially deamidated peptides.

Another region of the protein that was highly modified included the site of phosphorylation of Ser[122]. Residues 118−145 (YRLPSNVDQSALSCSLSADGMLTFSGPK) and 120−145 contained a heterogeneous mixture of modifications as suggested by peaks in our example peptide fingerprint (Figure 5C). Figure 5C shows peaks at *m*/*z* 2682 and 2698, which correspond to *m*/*z* values for cysteine-carboxyamidomethylated (CAM) peptide 120−145 in the absence and presence of an oxidized methionine, respectively. The cysteines are modified by iodoacetamide, which is a result of chemical modification during sample processing. The peak at *m*/*z* 3017 in Figure 5C corresponds to peptide 118−145 with CAM-cysteine and oxidized methionine. In 61% of our samples, a peak with a monoisotopic mass of *m*/*z* 2705, which is consistent with phosphorylation of peptide 120−145 but without CAM, was found (Table 3 and Figure 8). As noted, the cysteine in this peptide is not chemically modified by iodoacetamide. Incomplete chemical modification of cysteine during sample processing was observed in ∼50% of the peptides containing Cys[131]. These results are

Table 3: Summary of Modified Tryptic Peptides Identified by MALDI-TOF MS[a]

residues	MC[c]	sequence[d]	mass[b] theoretical	mass[b] experimental	ppm[e]
1−11	0	M(o)DVTIQHPWFK	1416.686	1416.681	3.5[f]
1−11	0	M(a)DVTIQHPWFK	1442.701	1442.702	0.2[f,g]
1−11	0	M(o,a)DVTIQHPWFK	1458.697	1458.698	1.0[f]
1−11	0	MDVT(p)IQHPWFK	1480.657	1480.683	17.2[f]
1−11	0	M(a)DVTIQ(d)HPWFK	1485.677	1485.702	17.0[h]
1−12	1	M(o)DVT(p)IQHPWFKR	1652.753	1652.763	3.2
1−12	1	M(o,a)DVT(p)IQHPWFKR	1694.764	1694.771	4.2
92−104[i]	0	DFVEIHGKHN(d)ERQ	1608.764	1608.783	11.5
120−145	0	LPSNVDQSALSC(c)SLSADGMLTFSGPK	2681.268	2681.275	2.8[f]
120−145	0	LPSNVDQSALSC(c)SLSADGM(o)LTFSGPK	2697.263	2697.275	4.5[f]
120−145	0	LPS(p)NVDQSALSCSLSADGMLTFSGPK	2704.213	2704.237	9.3[j]
118−145	1	YRLPSNVDQSALSC(c)SLSADGM(o)LTFSGPK	3016.427	3016.447	6.6[f]

[a] Following in-gel trypsin or AspN digestion of αA crysallin resolved by 2D gel electrophoresis, peptide fragments were analyzed on either a QSTAR Pulsar quadrupole or a QSTAR XL MALDI-TOF mass spectrometer. Internal calibration was performed using either peptides from trypsin autolysis or αA crystallin. [b] Theoretical and experimental masses are the monoisotopic molecular mass for the peptide plus the indicated modification(s). [c] MC is the number of trypsin- or ASPN-missed cleavage sites in the peptide. [d] Peptide sequence with the modification indicated in parentheses, positioned C-terminal to the relevant amino acid: a, acetylation (+42.010); c, *S*-carboxyamidomethylation of cysteine by iodoacetamide (+57.022); d, deamidation (+0.984); o, oxidation (+15.994); p, phosphorylation (+79.966). [e] Parts per million, calculated as [(theoretical − experimental)/theoretical] × 10^6. [f] Modified peptides shown in the spectrum of Figure 4. [g] Sequence verified by ESI tandem MS (Figure 6). [h] Mass values are following methyl esterification of the carboxy terminus (+14), D^2 (+14), and the deamidated Q^6 (+15). [i] AspN digestion. [j] Corresponds to the peptide shown in Figure 7.

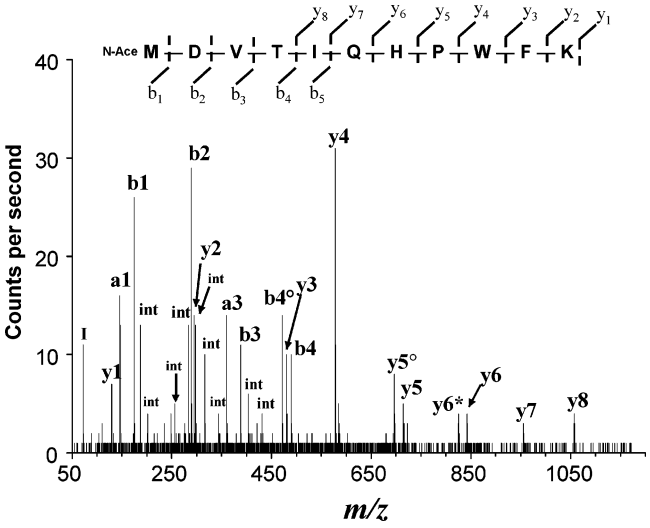

FIGURE 7: Product ion spectrum of the doubly charged ion 722.4 of *N*-acetylated (N-ace) peptide MDVTIQHPWFK from LC−MS. The amino acid sequence is displayed above the spectrum. The y- and b-type product ions found experimentally are written above and below the sequence, respectively. All b and y ions cannot be shown on spectrum because of space constraints. The asterisk denotes loss of NH_3, and the degree signs denote loss of H_2O from a fragment ion. Fragment ion nomenclature and neutral loss notation were established by Biemann (*76*). Our notation "int" denotes internal fragmentation, which is promoted by the presence of proline in the peptide sequence. Immonium ions are labeled globally with an I.

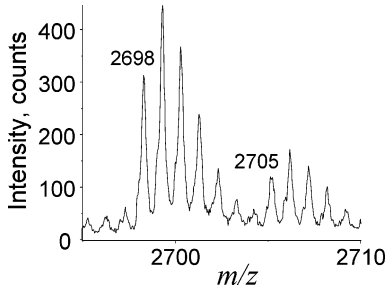

FIGURE 8: MALDI-TOF MS spectrum of tryptic peptides from αA crystallin containing post-translational modifications. Peptide 2698 from residues 120−145 (LPSNVDQSALSCSLADGMLTFSGPK) containing an oxidized methionine and *S*-carboxymethylation of cysteine. Peptide 2705 consists of residues 120−145 with an added phosphate. Mass accuracy between the theoretical and experimental values for this peptide is shown in Table 3.

consistent with our previous published work where we reported MS/MS sequencing of peptides containing a mixture of both chemically modified and unmodified cysteines that were present simultaneously in our samples (*46*).

Because we were not able to achieve the stringent level of mass accuracy required for definitive confirmation of the peptide with a phosphate, we turned to an alternative analysis to confirm the presence of a phosphorylated serine in our samples. Western immunoblotting was performed using an antibody that recognizes phosphoserine. We observed a positive immune reaction in the most abundant protein spot (spot 2) and also in the insert protein (spot I) (data not shown). On the basis of the faint immune reaction on our Western blots, the reaction of the antibody with a limited number of the αA crystallin spots can be explained by the either the low affinity of this antibody or the low abundance of phosphoserine. This is consistent with our mass spectral data, which showed a mixture of both phosphorylated and nonphosphorylated peptides in our samples. Thus, the cumulative evidence of peptides with masses consistent with phosphorylation of Ser^{122} and the positive immune reaction with a phosphoserine antibody strongly suggest Ser^{122} is phosphorylated in retinal αA crystallin. However, we acknowledge the potential for additional serine phosphorylation sites that are yet undescribed in this protein.

Other previously reported PTMs that would result in a more acidic migration included glycation (mass addition of *m*/*z* 162.05) of Lys^{11}, Lys^{78}, and Lys^{162} (*47*) and glutathionylation (mass addition of *m*/*z* 305.3) of Cys^{131} (*42*). We were unsuccessful in matching the theoretical mass of either the glycated or glutathionylated peptides with our observed mass values.

Table 2 provides a summary of the PTM and the putative modified residues for each protein spot. As observed from

the cumulative data, the N-terminus of retinal αA crystallin is highly modified and includes acetylation, deamidation, oxidation, and phosphorylation. Our mass spectral data provided evidence for phosphorylation of Thr^4 in spots 2−5 and I. Evidence for phosphorylation of Ser^{122} was observed in all spots except spot 5. It is possible that sites of phosphorylation in additional spots could have been missed due to incomplete sequence coverage and the inefficiency of phosphorylated peptides to ionize well in the positive ion mode or due to the low abundance of the phosphorylated protein in a mixture with the unphosphorylated protein in our samples.

In addition to the PTMs already described, T1 has been further modified by truncation. Evidence for the site of truncation at the N-terminus includes (1) the selective reaction with only the antibody that recognizes the last 10 amino acids in the C-terminus (Figures 3 and 4) and (2) the absence of peptides from the first 11 N-terminal residues in the mass fingerprint. The absence of a peptide in a peptide map may occur from signal suppression or inefficient ionization in a mixture, but since we have detected peptide 1−11 in mixtures of peptides from proteins other than T1, we expect that this peptide would ionize well in a mixture after digestion of T1. Peptides of residues 12−21 and 13−21 (an arginine at position 12 provides alternative cleavage sites) were present in the mass fingerprint. Truncation of the first 11 residues from the N-terminus would result in a protein of approximately the correct size predicted from the faster migration. The first 11 residues contain one positive charge (Lys^{11}) and four negative charges (Asp^2, deamidated Gln^6, and phosphorylated Thr^4), resulting in a net charge of −3. Removal of this portion of the protein would cause the truncated αA crystallin to migrate at a lower mass and a more basic pI than the parent protein. As observed on Western immunoblots (Figure 4), this migration is consistent with spot 2 being the parent protein since T1 migrates faster and at a more basic pI than this spot. Other truncated species that migrated at lower masses were found with the antibodies that recognize either the N- or C-terminus. However, because of the limited amount of protein in these spots, we were not able to obtain MS data for these samples.

DISCUSSION

Summary of Results. This study is the first to characterize αA crystallin content and PTM in the sensory retina. Our results show that retinal αA crystallin is highly modified. Evidence includes the presence of (1) αA crystallin in multiple protein spots with altered migration and (2) tryptic peptides with masses consistent with the addition of one or more modifications. These modifications include phosphorylation, deamidation, acetylation, and oxidation. Additionally, we show an age-related decrease in the level of protein expression and an altered pattern of N- and C-terminal truncation.

αA Crystallin Function. αA crystallin is a member of the small heat shock protein (HSP) family of proteins that function by sequestering unfolded polypeptides and preventing irreversible aggregation. Protein refolding is accomplished with other members of the HSP family, i.e., HSP 70 or HSP90, that associate with the α-crystallin−unfolding protein complex (*48*). Cellular conditions that initiate protein unfolding include elevated temperature, pH extremes, hypoxia, osmotic changes, noxious chemicals, and oxidative stress. In addition to the role as chaperone, α-crystallins have also demonstrated an ability to modulate actin polymerization in lens cells (*49*) and antiapoptotic activity in lens epithelial cells (*50*). The protection provided by αA crystallin under conditions conducive to protein unfolding or the initiation of apoptosis is determined by both the intracellular crystallin concentration and the extent of PTM, which has been shown in many cases to alter crystallin function (*18*).

Although the role of αA crystallin in the retina has not been fully investigated, evidence of its upregulation under conditions of light-induced retinal damage suggests it serves as one of the key chaperones in the retina (*39*). αA crystallin was first described in retinal photoreceptor cells from frogs, where it was shown to be present in the soluble fraction and also associated with the post-Golgi membranes (*4*). These observations led to the idea that αA crystallin was involved in the vectoral transport of rhodopsin from the Golgi to the newly assembling disks of the rod outer segments in the photoreceptor cell. Thus, a loss of chaperone activity through either a decreased content or an increased frequency of PTMs that alter function could have a detrimental effect on vision since rhodopsin is the major protein in the visual cascade.

Lenticular αA Crystallin. The consequence of disease and aging on αA crystallin structure and function has been most intensely studied in the lens. In this tissue, αA crystallin chaperone function is essential for maintenance of lens transparency. Definitive evidence for the *in vivo* function of this protein comes from mice with a targeted disruption of the αA crystallin gene. These knockout mice develop cataracts and inclusion bodies composed of αB crystallin, suggesting a role for αA crystallin in maintaining the solubility of the α-crystallin oligomeric complex (*51*). Additionally, cataracts have been associated with specific PTM that altered αA crystallin function. For example, C-terminal truncation of αA crystallin in diabetic lens leads to inhibited chaperone function and cataract formation (*52*). The occurrence of senile cataracts has also been associated with an age-related increase in the level of αA crystallin PTM and general loss of chaperone activity (*53*). For lenticular αA crystallin, the PTM reported to increase with aging includes deamidation, phosphorylation, acetylation, oxidation of methionine, and truncation of both the N- and C-termini (*12*, *20*−*22*, *24*). Furthermore, the increased fraction of high-molecular mass crystallin aggregates and decreased level of αA crystallin expression all contribute to a general loss in chaperone activity in the lens with aging (*23*, *54*−*58*).

Retinal αA Crystallin. To date, a detailed examination of specific age-related alterations in retinal crystallins has not been conducted. Since the retina is in a highly oxidative environment that experiences periodic hypoxia and osmotic changes, maintenance of crystallin function is crucial for protecting against irreversible aggregation of unfolding proteins. We asked if modifications similar to those described in lenticular αA crystallin also occurred in retinal αA crystallin. Our analytical strategy for identifying PTM in retinal αA crystallin was to search the MALDI-TOF mass fingerprints from tryptic digests for masses consistent with previously described modifications from lenticular αA crystallin. We were successful in finding many *m*/*z* values that

Table 4: Sequence Alignment of the N-Termini of αA and αB Crystallin Exhibiting a Positive Immune Reaction to an Antibody Generated to Residues 1−11 in Bovine (*5*, *6*)

Species	Sequence[a]	Accession #	Tissue
Bovine[b]	***MD*** IA***IQHPW***FK	NP 776714	kidney
Rat	***MD***VT***IQHPW***FK	NP 036666	heart, lung, intestine, spleen, skin, retina[c]
Human	***MD***VT***IQHPW***FK	NP 000385	lens (fetal to 80 years)
Pig	***MD*** IA***IQHPW***FK	P02475	kidney
αB (rat)	***MD*** IA***IHPW***I R	NP 037067	heart, lung, intestine, spleen, skin, retina[c]
αB (human)	***MD*** IA***IHPW***I R	P02511	lens (fetal to 80 years)

[a] Homologous regions common to all sequences are shown in italics. [b] Peptide used to generate the polyclonal antibody. The peptide contained an N-terminal acetylation. [c] Reaction in retinal crystallin is data from this research.

corresponded to modified peptides. However, most of our attempts to acquire high-quality tandem MS data for the modified peptides of interest failed, most likely due to a low signal-to-noise ratio, which reflects low abundance and/or poor ionization efficiency. Therefore, we performed internal calibration on all peptide map mass spectral data sets, which should theoretically bring "true" peptide *m*/*z* values closer to their theoretical number. Since we can prove with multiple tandem MS data sets that crystallin protein is in our sample, and the numbers for all of the potentially modified peptides came closer to the theoretical value after internal calibration, we feel that our strategy is well-founded. Statistically, some of the values for modified peptide masses would be expected to drift further away from the theoretical value if the numbers truly appear from contaminants or other undefined peptides and/or molecules that are not actually crystallin-derived peptides. Since all of our internally calculated values showed lower ppm compared with those same values we obtained with external calibration, we feel strongly about reporting the modified peptides in this paper. Our biochemical data and other data published on modified peptides from lens crystallin help support our argument. Thus, the analytical strategy presented here provides a sensitive method for determining both the type and site of PTM using *a priori* information.

Retinal Protein Content. Histological evaluation of the retina in aged pigmented rats has shown a 20−35% reduction in photoreceptor cell density compared with that in young rats (*40*, *41*). In this study, we measured the relative concentration of rhodopsin, a major constituent of photoreceptors, to estimate the extent of photoreceptor loss in our experimental animals. We found a 30% decrease in the concentration of rhodopsin, which is consistent with an age-dependent loss in photoreceptors observed by retinal morphological measurements.

The cellular location of α-crystallin has been investigated by immunohistochemistry and Western immunoblotting of isolated, specific retinal cells. The cells from the sensory retina demonstrating a positive immune reaction include photoreceptor cells, ganglion cells, Muller cells, and the inner nuclear layer containing horizontal, bipolar, and amacrine cells of the sensory retina (*4*, *39*, *59*−*62*). Thus, it appears that most retinal cells express α-crystallin, but the relative abundance among the different cell types has not been quantified. In our oldest animals, the difference between the content in αA crystallin and rhodopsin indicates that the age-dependent loss of photoreceptors does not completely account for the lower content of αA crystallin in the sensory retina. These results suggest there is an overall loss of αA crystallin content in all retinal cells.

An alternative explanation for the observed loss of αA crystallin content with aging could be that the decreased solubility of αA crystallin could cause preferential sedimentation and loss during our sample preparation. Thus, it should be emphasized that our data reflect the soluble content of αA crystallin. Additionally, we emphasize that our measurements of content were performed on the intact protein, and therefore, truncated species would not be included in the total content. Using antibodies that recognize either the N- or C-terminus, we were able to show by 2D gel resolution that there was more N-terminal truncation in aged retina than in retina from the younger age groups. In contrast, there is no detectable C-terminal truncation within our oldest age group. C-Terminal truncation was evaluated using an antibody generated to the first 11 residues of bovine αA crystallin, a region that contains multiple PTMs. It is possible that these PTMs could alter the immune reaction and provide ambiguous results. To address this possibility, we performed a sequence alignment of the N-terminus of αA and αB crystallin from species with a reported positive immune reaction to this antibody (Table 4) (refs *5* and *6* and data from this study). There was a high degree of sequence homology between species and also between αA and αB crystallin. Comparison of the regions of variable amino acids suggests that residues 3, 4, 6, 10, and 11 are not crucial for antibody recognition since different amino acids can be substituted yet the antibody still binds. Thus, modification of Thr^4 and Gln^6 would likely not interfere with antibody binding. The other site of modification in retinal αA crystallin is Met^1. Acetylation of Met^1 was part of the immunogenic peptide and therefore may be part of the recognition signal. At this time, it is unclear how oxidation of Met^1 could affect antibody binding. Although these age-dependent differences in truncation could slightly alter our estimates of relative content, we feel confident that the final conclusions would still be the same.

Since the content of a specific protein reflects the balance between synthesis and degradation, one must conclude that the mechanism behind the lower content of αA crystallin is either slower protein synthesis or accelerated protein degradation. In this study, we did not examine these two potential mechanisms. However, in a previous study, we showed that the function of the proteasome, the protease responsible for degradation of most intracellular proteins, is significantly inhibited in aged retina (*28*). Whether αA crystallin is an *in vivo* substrate for the proteasome has not

yet been confirmed but appears to be likely on the basis of the ubiquitous nature of this protease. Therefore, we feel that accelerated degradation of αA crystallin is probably not the mechanism behind the lower content with aging. Further studies will be required for more conclusive statements to be made.

Another interesting observation was the high content of αA insert found in the retina. In the lens, αA insert is only a minor product, with mRNA being expressed in 10−20% of αA crystallin (*38*). These estimates are consistent with the 6−8-fold difference in relative protein levels for αA crystallin and αA insert in mouse lens resolved by 2D electrophoresis (*22*). In contrast to the lens where αA insert is a minor component, the retinal αA insert content was ∼50−70% of to the αA crystallin content in adult and middle age rats when retinal proteins were separated on 1D gels (Figure 1). Additionally, our results show a significant decrease in the level of expression of both αA crystallin and αA insert in the oldest age group. This result again contrasts with evidence in the lens, where no age-related differences in either the ratio of mRNA or the polypeptides were found (*38*).

While it has been shown that αA insert is an integral part of the rodent αA complex (*63*), there have been conflicting reports about the functional consequences of this protein. For example, homopolymers of αA insert have demonstrated 4−5-fold less activity than homopolymers of αA crystallin (*64*). In another study, multimeric αA insert demonstrated thermostability and structure similar to those of multimers of αA crystallin (*38*). Thus, it is still unclear whether the presence of αA insert provides a functional advantage and, even more interestingly, why this protein product has been selectively retained in the rodent eye and is found in such great abundance in the retina.

Following 2D gel separation, the amount of αA insert relative to αA crystallin was reduced by at least 50% (Figure 4). This observation may provide important clues about the subcellular localization or protein association of αA insert. One explanation for the discrepancy between 1D and 2D separation techniques could be that the αA insert proteins are tightly associated with retinal membranes or the less soluble cytoskeleton and therefore do not solubilize sufficiently for resolution on 2D gels. In support of this idea, association between α-crystallin and both membranes and intermediate beaded filaments of the cytoskeleton has been demonstrated (*65*, *66*). Another possibility is that retinal αA insert has a greater propensity to form insoluble aggregates that are only dissociated in the presence of an anionic detergent, like SDS, that is used with 1D electrophoresis.

PTM Alters the Intrinsic Charge. The presence of multiple protein spots resolved on 2D gels that were identified as αA crystallin is a clear indication of PTM (Figure 4). αA crystallin with altered migration in both the first and second dimension was also noted in lens from mice and humans (*20*, *22*). In both studies, multiple spots were observed even at very young ages, indicating this protein is readily modified. However, there was an obvious age-dependent increase in the number of spots corresponding to αA crystallin, suggesting PTMs accumulate or occur at an accelerated rate with aging.

In our rat retinal samples, migration of the five major spots was between pI 5.4 and 6.5. Spot 2, the major species, migrated at a pI that is more basic than the theoretical pI of 5.77. The discrepancy between the theoretical and experimental pI for rat retinal αA crystallin could potentially be due to other yet undefined PTMs that result in a protein with a more basic charge. Support for additional PTM includes (1) a number of clearly resolved peaks on our spectra that we were not able to match to a peptide from αA crystallin, trypsin, or keratin contaminants, (2) similar modifications that were found in each protein spot (so the currently identified PTM could not account for the change in migration), and (3) incomplete sequence coverage (so additional PTM could have escaped our detection). An important question that needs to be addressed is whether there are PTMs that are unique to the retina, thus reflecting a difference in the cellular environment, or if PTMs are similar in all crystallins regardless of the tissue.

Specific PTMs that have been described in lenticular αA crystallin that alter the intrinsic charge include phosphorylation, deamidation, glycation and acetylation of lysine, and glutathionylation. These modifications give rise to a protein with a more acidic migration. In rat retinal αA crystallin, we found evidence for phosphorylation and deamidation. Phosphorylation of Ser^{122}, the major site of *in vivo* phosphorylation that occurs via cAMP-dependent protein kinase pathways, was found in three major spots (*66*). Phosphorylation of Thr^4, a site that is responsive to oxidative and calcium-induced stress in lens epithelial cells, was found in all major spots (*44*). To the best of our knowledge, this is the first report of Thr^4 phosphorylation in αA crystallin isolated from a tissue. The sequence surrounding Thr^4 is not a recognition motif for any of the known kinases, so the identity of the kinase responsible for phosphorylation is still unknown. For both Ser^{122} and Thr^4, no age-dependent differences in phosphorylation were noted. The functional consequences of phosphorylation currently remain controversial since there are conflicting reports of no change or an improvement in chaperone activity in the literature (*45*, *68*).

Deamidation of asparagine and glutamine residues is one of the most prevalent PTMs that occurs in the aging lens. This modification alters the local charge, which can destabilize protein structural integrity and alter function. In our samples, we found deamidation of Gln^6 and Asn^{101}, which are modifications previously reported in the lens (*19*, *21*, *69*). Asn^{101} deamidation is a common modification in the lens that occurs in ∼45% of younger donors and is modified in ∼50% of older (>30 years) donors (*69*).

Oxidation of Met to methionine sulfoxide was found consistently in our samples for Met^1 and Met^{138}. This modification does not alter the intrinsic charge, and therefore should be "silent" with regard to its effect on protein mobility. Although it is uncertain if these modifications occurred *in vivo* or as a result of sample preparation, the observation of Met^1 oxidation using two different non-gel-based methods of sample preparation, i.e., elution from a membrane and multidimensional liquid chromatography, followed by MS analysis suggests the *in vivo* origin of this modification (*70*, *71*). Oxidation of Met^{138} has also been reported by others (*71*).

Truncation. Truncation of αA crystallin is a common feature of aging in the lens. As we have shown here, truncation also occurs in the retina, although to a lesser extent than in the lens. In the lens, calpains and Lp82, a lens specific

protease, have demonstrated site specific cleavage of αA crystallin (*72*). In the retina, calpains and the retina-specific Rt88, a protein homologue of Lp82, may be involved in retinal αA crystallin truncation (*73*). The most prevalent truncation reported in the lens is from the C-terminus and includes elimination of 1−22 amino acids (*20*, *21*, *24*, *72*). To investigate the functional consequences of C-terminal truncation, site-directed mutagenesis was used to delete the last 17 amino acids (*16*). These mutant αA crystallin proteins formed large aggregates and had inhibited chaperone function. C-Terminal truncation by limited proteolysis produced a protein with a reduced ability to protect against heat-induced denaturation (*8*). In our retinal homogenates, we detected αA crystallin with C-terminal truncations mainly in adult and middle age rats, but not in the oldest age group. The absence of C-terminal truncation in the oldest age group could be a result of an age-related loss in function of the proteases responsible for the truncations. Alternatively, the truncated species could be degraded more quickly in the oldest group.

In our retinal samples, we did observe N-terminal truncation of retinal αA crystallin that was present in all ages, but more prominent in retina from old rats. These results are consistent with reports of an increased level of N-terminal cleavage in the aged lens (*12*, *74*). A role for the hydrophobic N-terminus in chaperone function was previously suggested (*8*, *75*). A recent study that engineered chimeric proteins by swapping the N-terminal domains of αA crystallin and αB crystallin lends support for the importance of the N-terminus in αA crystallin chaperone function (*76*). In these studies, the engineered protein containing the N-terminal domain of αA crystallin had enhanced chaperone activity, whereas the chimera containing the αB crystallin N-terminal domain exhibited a complete loss of chaperone function. Taken together, these results highlight the detrimental functional consequences of truncation in either the N- or C-terminus. Therefore, the age-dependent increase in the level of N-terminal truncation that we observed suggests compromised function of αA crystallin in the aged retina.

CONCLUSIONS

Our analyses were performed on the sensory retina. This tissue is composed of a heterogeneous population of seven cell types that are, with the exception of the photoreceptors, postmitotic, i.e., experience minor cell replacement (*26*). Unlike proteins in the lens fiber cell that do not turn over, retinal proteins are continuously replaced. Therefore, the observation that retinal αA crystallin contains PTMs similar to those reported in the lens suggests the modifications are not due to the long lifetime of αA crystallin but rather may reflect the protein's intrinsic sensitivity to damage from environmental insult. The correlation between PTM and loss of chaperone function in lens crystallin suggests retinal crystallin may also experience a modification-induced loss of chaperone function. The consequences of these PTMs for retinal survival are still unresolved. However, it is likely that the protection provided by the α-crystallins is an important mechanism for coping with a variety of stresses. Additionally, we did find some substantial tissue specific differences, such as the higher content of αA insert, fewer truncations, and a mixture of acetylated and nonacetylated N-terminal peptides in the retina. Furthermore, the presence of PTMs that we observed does not fully explain the difference in the migration of individual protein spots. Therefore, it is probable that additional PTMs occur in retinal αA crystallin. Nonetheless, the decreased level of expression and altered truncation of αA crystallin that we describe in the aged retina suggest protection from stress-induced protein aggregation is compromised with aging. A loss of chaperone function may be mechanistically linked to the sharp decline in vision observed later in life.

ACKNOWLEDGMENT

We thank J. Mark Petrash for human recombinant αA crystallin, Joseph Horwitz for αA crystallin antibody, and Dale Gregerson for insightful discussion. We acknowledge the Mass Spectrometry Consortium for the Life Sciences, University of Minnesota, St. Paul, MN, for the assistance in acquisition and interpretation of mass spectral data.

REFERENCES

1. Horowitz, J. (1992) Alpha crystallin can function as a molecular chaperone, *Proc. Natl. Acad. Sci. U.S.A. 89*, 10449−10453.
2. Overbeek, P. A., Chepelinsky, A. B., Khillan, J. S., Piatigorsky, J., and Westphal, H. (1985) Lens-specific expression and developmental regulation of the bacterial chloramphenicol acetyltransferase gene driven by the murine alpha A-crystallin promoter in transgenic mice, *Proc. Natl. Acad. Sci. U.S.A. 82*, 7815−7819.
3. Kato, K., Shinohara, H., Kurobe, N., Goto, S., Inaguma, Y., and Ohshima, K. (1991) Immunoreactive αA-crystallin in rat non-lenticular tissues detected with a sensitive immunoassay method, *Biochim. Biophys. Acta 1080*, 173−180.
4. Deretic, D., Aebersold, R. H., Morrison, H. D., and Papermaster, D. S. (1994) αA- and αB-crystallin in the retina, *J. Biol. Chem. 269*, 16853−16861.
5. Srinivasan, A. N., Nagineni, C. N., and Bhat, S. P. (1992) Alpha A crystallin is expressed in non-ocular tissues, *J. Biol. Chem. 267*, 23337−23341.
6. Bhat, S. P., Horwitz, J., Srinivasan, A., and Ding, L. (1991) αB-Crystallin exists as an independent protein in the heart and in the lens, *Eur. J. Biochem. 102*, 775−781.
7. Derham, B. K., and Harding, J. J. (1999) α-Crystallin as a molecular chaperone, *Prog. Retinal Eye Res. 18*, 463−509.
8. Takemoto, L., Emmons, T., and Horwitz, J. (1993) The C-terminal region of α-crystallin: involvement in protection against heat-induced denaturation, *Biochem. J. 294*, 435−438.
9. Kuehn, M. J., Ogg, D. J., Kihlberg, J. S., Slonim, L. N., Flemmer, K., Bergfors, T., and Hultgren, S. J. (1993) Structural basis of pilus subunit recognition by the PapD chaperone, *Science 262*, 1234−1241.
10. Sharma, K. K., Kumar, R. S., Kuman, G. S., and Quinn, P. T. (2000) Synthesis and characterization of a peptide identified as a functional element in αA crystallin, *J. Biol. Chem. 275*, 3767−3771.
11. Berengian, A. R., Bova, M. P., and Mchaourab, H. S. (1997) Structure and function of the conserved domain in αA-crystallin. Site-directed spin labeling identifies a β-strand located near a subunit interface, *Biochemistry 36*, 9951−9957.
12. Kamei, A., Iwase, H., and Masuda, K. (1997) Cleavage of amino acid residue(s) from the N-terminal region of αA- and αB-crystallins in human crystalline lens during aging, *Biochem. Biophys. Res. Commun. 231*, 373−378.
13. Bera, S., Thampi, P., Cho, W. J., and Abraham, E. C. (2002) A positive charge preservation at position 116 of αA-crystallin is critical for its structural and functional integrity, *Biochemistry 41*, 12421−12426.
14. Smulders, R. H., Merck, K. B., Aendekerk, J., Horwitz, J., Takemoto, L., Slingsby, C., Bloemendal, H., and de Jong, W. W. (1995) The mutation Asp69 → Ser affects the chaperone-like activity of αA-crystallin, *Eur. J. Biol. Chem. 232*, 834−838.
15. Plater, M. L., Goode, D., and Crabbe, M. J. (1996) Effects of site-directed mutations on the chaperone-like activity of αB-crystallin, *J. Biol. Chem. 271*, 28558−28566.

16. Andley, U. P., Mathur, S., Griest, T. A., and Petrash, J. M. (1996) Cloning, expression, and chaperone-like activity of human αA-crystallin, *J. Biol. Chem. 271*, 31973−31980.
17. Derham, B. K., and Harding, J. J. (2002) Effects of modifications of α-crystallin on its chaperone and other properties, *Biochem. J. 362*, 711−717.
18. Groenen, P. J., Merck, K. B., de Jong, W. W., and Bloemendal, H. (1994) Structure and modifications of the junior chaperone α-crystallin. From lens transparency to molecular pathology, *Eur. J. Biochem. 225*, 1−19.
19. Miesbauer, L. R., Zhou, X., Yang, Z., Yang, Z., Sun, Y., Smith, D. L., and Smith, J. B. (1994) Post-translational modifications of water-soluble human lens crystallins from young adults, *J. Biol. Chem. 269*, 12494−12502.
20. Colvis, C., and Garland, D. (2002) Posttranslational modification of human αA-crystallin: correlation with electrophoretic migration, *Arch. Biochem. Biophys. 397*, 319−323.
21. Hanson, S. R. A., Hasan, A., Smith, D. L., and Smith, J. B. (2000) The major *in vivo* modifications of the human water-insoluble lens cystallins are disulfide bonds, deamidation, methionine oxidation and backbone cleavage, *Exp. Eye Res. 71*, 195−207.
22. Ueda, Y., Duncan, M. K., and David, L. L. (2002) Lens proteomics: the accumulation of crystallin modifications in the mouse lens with age, *Invest. Ophthalmol. Visual Sci. 43*, 205−213.
23. Takemoto, L., and Boyle, D. (1994) Molecular chaperone properties of the high molecular weight aggregate from aged lens, *Curr. Eye Res. 13*, 35−44.
24. Takemoto, L., and Gopalakrishnan, S. (1994) Alpha-A crystallin: quantitation of C-terminal modification during lens aging, *Curr. Eye Res. 13*, 879−883.
25. Fliesler, S. J., and Anderson, R. E. (1983) Chemistry and metabolism of lipids in the vertebrate retina, *Prog. Lipid Res. 22*, 79−131.
26. Gordon, W. C., and Bazan, N. G. (1997) Retina, in *Biochemistry of the Eye* (Harding, J. J., Ed.) pp 144−275, Chapman and Hall Medical, London.
27. Rozanowska, M., Jarvis-Evans, J., Korytowski, W., Boulton, M. E., Burke, J. M., and Sarna, T. (1995) Blue light-induced reactivity of retinal age pigment. *In vitro* generation of oxygen-reactive species, *J. Biol. Chem. 270*, 18825−18830.
28. Louie, J. L., Kapphahn, R. J., and Ferrington, D. A. (2002) Proteasome function and protein oxidation in the aged retina, *Exp. Eye Res. 75*, 271−284.
29. Laemmli, U. K. (1970) Cleavage of structural proteins during the assembly of the head of bacteriophage T4, *Nature 227*, 680−685.
30. Shevchenko, A. M., Wilm, M., Vorm, O., Jensen, O. N., Podtelejnikov, A. V., and Neubauer, G. (1996) A strategy for identifying gel-separated proteins in sequence database by MS alone, *Biochem. Soc. Trans. 24*, 893−896.
31. Jensen, O. N., Wilm, M., Shevchenko, A., and Mann, M. (1999) Sample preparation methods for mass spectrometric peptide mapping directly from 2-DE gels, in *2-D Proteome analysis protocols* (Lenk, A. J., Ed.) pp 513−527, Humana Press, Totowa, NJ.
32. Goodlett, D. R., Keller, A., Watts, J. D., Newitt, R., Yi, E. C., Purvine, S., Eng, J. K., von Haller, P., Aebersold, R., and Kolker, E. (2001) Differential stable isotope labeling of peptides for quantitation and de novo sequence derivation, *Rapid Commun. Mass Spectrom. 15*, 1214−1221.
33. Hernandez, V. P., Higgins, L., and Fallon, A. M. (2003) Characterization and cDNA cloning of an immune-induced lysozyme from cultured *Aedes albopictus* mosquito cells, *Dev. Comp. Immunol. 27*, 11−20.
34. Wilkins, M. R., Gasteiger, E., Cooley, A., Herbert, B., Molloy, M. P., Binz, P. A., Ou, K., Sanchez, J. C., Bairoch, A., Williams, K. L., and Hochstrasser, D. F. (1999) High-throughput mass spectrometric discovery of protein post-translational modifications, *J. Mol. Biol. 289*, 645−657.
35. Turturro, A., Witt, W. W., Lewis, S., Hass, B. S., Lipman, R. D., and Hart, R. W. (1999) Growth curves and survival characteristics of the animals used in the biomarkers of aging program, *J. Gerontol. 54A*, B492−B501.
36. Caspers, G. J., Pennings, J., and de Jong, W. W. (1994) A partial cDNA sequence corrects the human αA-crystallin primary structure, *Exp. Eye Res. 59*, 125−126.
37. de Jong, W. W., Cohen, L. H., Leunissen, J. A., and Zweers, A. (1980) Internally elongated rodent α-crystallin A chain: resulting from incomplete RNA splicing? *Biochem. Biophys. Res. Commun. 96*, 648−655.
38. King, C. R., and Piatigorsky, J. (1984) Alternative splicing of αA crystallin in RNA, *J. Biol. Chem. 259*, 1822−1826.
39. Sakaguchi, H., Miyagi, M., Darrow, R. M., Crabb, J. S., Hollyfield, J. G., Organisciak, D. T., and Crabb, J. W. (2003) Intense light exposure changes the crystallin content in retina, *Exp. Eye Res. 76*, 131−133.
40. Weiss, I. (1995) Changes in the aging rat retina, *Ophthalmic Res. 27*, 154−163.
41. Katz, M. L., and Robison, G. R. (1986) Evidence of cell loss from the rat retina during senescence, *Exp. Eye Res. 42*, 293−304.
42. Cherian, M., Smith, J. B., Jiang, X. Y., and Abraham, E. C. (1997) Influence of protein-glutathione mixed disulfides on the chaperone-like function of alpha-crystallin, *J. Biol. Chem. 272*, 29099−29103.
43. Clauser, K. R., Baker, P., and Burlingame, A. L. (1999) Role of accurate mass measurement (±10 ppm) in protein identification strategies employing MS or MS/MS and database searching, *Anal. Chem. 71*, 2871−2882.
44. Wang, K., Gawinowicz, M. A., and Spector, A. (2000) The effect of stress on the pattern of phosphorylation of αA and αB crystallin in the rat lens, *Exp. Eye Res. 71*, 385−393.
45. Wang, K., Ma, W., and Spector, A. (1995) Phosphorylation of alpha-crystallin in rat lenses is stimulated by H_2O_2 but phosphorylation has no effect on chaperone activity, *Exp. Eye Res. 61*, 115−124.
46. Bennaars-Eiden, A., Higgins, L., Hertzel, A. V., Kapphahn, R. J., Ferrington, D. A., and Bernlohr, D. A. (2002) Covalent modification of epithelial fatty acid binding protein by 4-hydroxynonenal in vitro and in vivo, *J. Biol. Chem. 277*, 50693−50702.
47. Abraham, E. C., Cherian, M., and Smith, J. B. (1994) Site selectivity in the glycation of αA- and αB-crystallins by glucose, *Biochem. Biophys. Res. Commun. 201*, 1451−1456.
48. Wang, K., and Spector, A. (2000) Alpha-crystallin prevents irreversible protein denaturation and acts cooperatively with other heat shock proteins to renature and stabilize partially denatured protein in an ATP-dependent manner, *Eur. J. Biochem. 267*, 4705−4712.
49. Wang, K., and Spector, A. (1996) Alpha-crystallin stabilizes actin filaments and prevents cytochalasin-induced depolymerization in a phosphorylation-dependent manner, *Eur. J. Biochem. 242*, 56−66.
50. Andley, U. P., Song, Z., Wawrousek, F. F., Fleming, T. P., and Bassnett, S. (2000) Differential protective activity of alpha A and alpha B crystallin in lens epithelial cells, *J. Biol. Chem. 275*, 36823−36831.
51. Brady, J. P., Garland, D., Duglas, Y., Robison, W. G., Groome, A., and Wawrousek, E. F. (1997) Targeted disruption of the mouse αA crystallin gene induces cataract and cytoplasmic inclusion bodies containing the small heat shock protein αB crystallin, *Proc. Natl. Acad. Sci. U.S.A. 94*, 884−889.
52. Thampi, P., Hassan, A., Smith, J. B., and Abraham, E. C. (2002) Enhanced C-terminal truncation of αA and αB crystallins in diabetic lens, *Invest. Ophthalmol. Visual Sci. 43*, 3265−3272.
53. Takemoto, L., Granstrom, D., Kodama, T., and Wong, R. (1988) Covalent change in alpha crystallin during senile cataractogenesis, *Biochem. Biophys. Res. Commun. 150*, 987−995.
54. Swamy, M. S., and Abraham, E. C. (1987) Lens protein composition, glycation and high molecular weight aggregation in aging rats, *Invest. Ophthalmol. Visual Sci. 28*, 1693−1701.
55. Yang, Z., Chamorro, M., Smith, D. L., and Smith, J. B. (1994) Identification of the major components of the high molecular weight crystallins from old human lens, *Curr. Eye Res. 13*, 415−421.
56. Swamy, M. S., and Abraham, E. C. (1991) Reverse-phase HPLC analysis of human α crystallin, *Curr. Eye Res. 10*, 213−220.
57. Horowitz, J., Emmons, T., and Takemoto, L. (1992) The ability of lens alpha crystallin to protect against heat-induced aggregation is age-dependent, *Curr. Eye Res. 11*, 817−822.
58. Cherian, M., and Abraham, E. C. (1995) Decreased molecular chaperone property of alpha crystallins due to posttranslational modifications, *Biochem. Biophys. Res. Commun. 208*, 675−679.
59. Maeda, A., Ohguro, H., Maeda, T., Nakagawa, T., and Kuroki, Y. (1999) Low expression of αA crystallin and rhodopsin kinase of photoreceptors in retinal dystrophy rat, *Invest. Ophthalmol. Visual Sci. 40*, 2788−2794.

60. Lewis, G. P., Kaska, D. D., Vaughan, D. K., and Fisher, S. K. (1988) An immunocytochemical study of cat retinal Müller cells in culture, *Exp. Eye Res. 47*, 855−868.
61. Simirskii, V. N., and Aleinikova, K. S. (2002) The 23-kDa polypeptide from common frog lens: isolation, characterization and cellular localization, *Ontogenez 33*, 276−284.
62. Xi, J., Farjo, R., Yoshida, S., Kern, T. S., Swaroop, A., and Andley, U. P. (2003) A comprehensive analysis of the expression of crystallins in mouse retina, *Mol. Vision 9*, 410−419.
63. Hendriks, W., Weetnik, H., Voorter, C. E. M., Sanders, J., Bloemendal, H., and de Jong, W. W. (1990) The alternative splicing product αA ins-crystallin is structurally equivalent to αA and αB subunits in the rat α-crystallin aggregate, *Biochim. Biophys. Acta 1037*, 58−64.
64. Smulders, R. H., van Geel, I. G., Gerards, W. L., Bloemendal, H., and de Jong, W. W. (1995) Reduced Chaperone-like Activity of αA ins-crystallin, an Alternative Splicing Product Containing a Large Insert Peptide, *J. Biol. Chem. 270*, 13916−13924.
65. Boyle, D. L., and Takemoto, L. (1996) EM immunolocalization of alpha crystallins: association with the plasma membrane from normal and cataractous human lens, *Curr. Eye Res. 15*, 577−582.
66. Fitzgerald, P. G., and Graham, D. (1991) Ultrastructural localization of alpha A crystallin to the bovine lens fiber cell cytoskeleton, *Curr. Eye Res. 10*, 417−436.
67. Spector, A., Chiesa, R., Sredy, J., and Garner, W. (1985) cAMP-dependent phosphorylation of bovine lens alpha-crystallin, *Proc. Natl. Acad. Sci. U.S.A. 82*, 4712−4716.
68. van Boekel, M. A., Hoogakker, S. E., Harding, J. J., and de Jong, W. W. (1996) The influence on some post-translational modifications on the chaperone-like activity of alpha crystallin, *Ophthalmic Res. 28*, 32−38.
69. Takemoto, L. J. (1998) Quantitation of asparagine-101 deamidation from alpha-A crystallin during aging of the human lens, *Curr. Eye Res. 17*, 247−250.
70. MacCoss, M. J., McDonald, W. H., Saraf, A., Sadygov, R., Clark, J. M., Tasto, J. J., Gould, K. L., Wolters, D., Washburn, M., Weiss, A., Clark, J. I., and Yates, J. R. (2002) Shotgun identification of protein modifications from protein complexes and lens tissue, *Proc. Natl. Acad. Sci. U.S.A. 99*, 7900−7905.
71. Takemoto, L., Horwitz, J., and Emmons, T. (1992) Oxidation of the N-terminal methionine of lens αA crystallin, *Curr. Eye Res. 11*, 651−655.
72. Ueda, Y., Fukiage, C., Shih, M., Shearer, T. R., and David, L. L. (2002) Mass measurements of C-terminally truncated α-crystallins from two-dimensional gels identify Lp82 as a major endopeptidase in rat lens, *Mol. Cell. Proteomics 1*, 357−365.
73. Azuma, M., Fukiage, C., Higashine, M., Nakajima, T., Ma, H., and Shearer, T. R. (2000) Identification and characterization of a retina-specific calpain (Rt88) from rat, *Curr. Eye Res. 21*, 710−720.
74. Lund, A. L., Smith, J. B., and Smith, D. L. (1996) Modifications of the water-insoluble human lens α crystallin, *Exp. Eye Res. 63*, 661−672.
75. Smith, J. B., Liu, Y., and Smith, D. L. (1996) Identification of possible regions of chaperone activity in lens alpha-crystallin, *Exp. Eye Res. 63*, 125−128.
76. Kumar, L. V., and Rao, C. M. (2000) Domain swapping in human αA and αB crystallin affects oligomerization and enhances chaperone-like activity, *J. Biol. Chem. 275*, 22009−22013.
77. Biemann, K. (1988) Contributions of mass spectrometry to peptide and protein structure, *Biomed. Environ. Mass Spectrom. 16*, 99−111.
78. Baldwin, M. A., Medzihradszky, D. F., Lock, C. M., Fisher, B., Settineri, T. A., and Burlingame, A. L. (2001) Matrix-assisted laser desorption/ionization coupled with quadrupole/orthogonal acceleration time-of-flight mass spectrometry for protein discovery, identification, and structural analysis, *Anal. Chem. 73*, 1707−1720.

BI034774E